DESCENT TRAJECTORY OPTIMIZATION FOR SOFT LUNAR LANDINGS

by

Maxwell Mason and Samuel M. Brainin
Hughes Aircraft Company

Presented at the
IAS 30th Annual Meeting
New York, New York
January 22-24, 1962

IAS Paper No. 62-11

~~Member Price - . . . $0.50~~
~~Nonmember Price - $1.00~~

DESCENT TRAJECTORY OPTIMIZATION FOR SOFT LUNAR LANDINGS

Maxwell Mason and Samuel M. Brainin
Aerospace Group, Space Systems Division
Hughes Aircraft Company

INTRODUCTION

On approach to an airless planet, such as the moon, the slowdown from approach speed to a soft-landing speed must be accomplished entirely by an on-board propulsion system, since no aerodynamic drag is available for this purpose. The minimum approach, or unslowed impact speed is the escape velocity, which for the moon is 7780 feet per second. An additional speed of the order of 1000 feet per second is usually desirable in order to shorten the transit time and to tailor that time so the lunar landing occurs when the moon is visible from chosen locations on the earth. By a soft landing is meant a speed of about 10 to 15 feet per second, implying a maximum deceleration on impact of 10 to 15 earth g. Thus, the retro engine system must take out some 9000 feet per second of velocity. The importance of efficient design of the descent maneuver and of the retro system can be emphasized by stating that approximately 75 percent of the injected spacecraft weight is devoted to the retro system. Of this 75 percent, 90 percent is fuel. A small fractional change in retro system weight therefore represents a very large fractional change in payload weight.

The design and optimization of the descent trajectory for minimum retro system weight is considered here for an unmanned vehicle. The design procedure is not a theoretical one with, for example, 'n' propulsion stages and a calculus of variations optimization. Instead, the major characteristics of the retro system are chosen from a practical hardware consideration of simple, reliable engines and instruments which exist today. Once chosen, the practical limitations of these components impose constraints on the system, and it is within these engineering constraints that the optimization procedure is performed.

In Part I of this paper, the physics of the procedure is emphasized, not the mathematics. In fact, Part I illustrates the procedure in general under the simplifying assumptions that 1) the trajectories are vertical, without velocity and attitude direction being considered as variables, and 2) the gravity field is constant. Under these assumptions, the mathematics are very simple since the equations of motion are integrable in closed form and a linear derivative technique performs the error analysis. The effects resulting from considering trajectory and thrust attitude angles off vertical as variables are mentioned briefly in Part I. The detailed method of handling the optimization procedure for machine computation in this more complicated case appears in Part II.

PART I. ENGINEERING DESIGN AND OPTIMIZATION OF TRAJECTORIES

1. MAJOR DESIGN CONSIDERATIONS

It is well known that for ideal efficiency a slowdown in a gravity field should be made at maximum thrust for minimum time and that the maneuver should start at an altitude where essentially zero velocity is reached at precisely the moon's surface. Such a maneuver requires resistance to unlimited acceleration and perfect sensing and control of the trajectory. In a practical attempt to approach this maneuver, a high-level, controllable thrust engine is indicated. This controllability demands a liquid propellant engine. For comparable engine weight, however, present liquid propellant engines have one-third the thrust level of solid propellant engines. This lower thrust level is less efficient in itself and also requires ignition at a much higher altitude, therefore necessitating much heavier instrumentation. For an unmanned vehicle at distances close to the moon, the greater accuracy and faster action of a control system which responds automatically to local sensing devices is preferable to one relying on tracking information and command from the earth.

For the major portion of the slowdown, a high constant-thrust, solid-propellant engine is desirable. Since this engine is not controllable, altitude and velocity dispersions will result at burnout. The nominal burnout, therefore, must occur at an altitude

high enough to ensure that a second, controllable, liquid-propellant engine, responding to local sensing, can remove the remaining, relatively small velocity before impact occurs.

Figure 1 illustrates typical descent trajectory behavior. In this figure and the following figures, however, the trajectory is not pictured in space, since, although the ordinate is altitude, the abscissa is velocity, downward to the right, upward to the left. The actual trajectories are to be considered vertical. For off-vertical approaches, the ordinate can be regarded as range and the abscissa as range rate. This approximation is good, since in the case of off-vertical trajectories with thrust direction closely opposing velocity direction, the angle of approach changes very little until very low speeds are reached.

In Figure 1, the dashed line to the right represents an approach trajectory without slowdown, the velocity increasing slightly as the vehicle falls to the moon. The solid curve represents the trajectory during main retro slowdown. As the trajectory proceeds, there is less altitude loss for two reasons: 1) the average speed is lower, and 2) for a near-constant thrust engine, the acceleration is greater since mass is decreasing. The dashed line in the center represents a fall from a midvalue of velocity. Note that now the increase of speed for a given altitude drop is greater than for the unslowed vehicle. Since the average speed is less, more time is spent in falling through a given height, and more time in a gravity field means more speed increase. This increase in speed must always be taken out if a soft landing is to be accomplished.

Toward the left in Figure 1, the fall starting at a low downward velocity exhibits a large speed increase in a small altitude drop. Indicated at the extreme left is the absurdity of having such a large impulse engine that the velocity at burnout is upward. The vehicle coasts upward, slowing down, then falls from a greater height acquiring even more speed before impact.

One possible simple concept for the second vernier engine maneuver is illustrated by the vertical dot-dash curve. Here the second engine simply holds a thrust level equal to lunar weight so that the descent from main retro burnout is made at the constant low landing speed. Such a maneuver is good and will be adopted at the very end of the descent, the final drop of a few tens of feet. But the maneuver is poor for the whole descent from main retro burnout for two reasons: 1) the velocity dispersion at main burnout, as will be shown, is too large to accept as a landing speed range, and 2) the altitude dispersion is large enough that even if the burnout speed were corrected by the vernier engine to the low landing speed soon after main burnout, the fall at this low constant speed through the remaining altitude at vernier thrust equal to lunar weight would be very costly in vernier engine fuel.

The desired trajectory after main retro burnout results from the same considerations which governed the main retro slowdown. It is best to drop as quickly as possible to an altitude and velocity condition, sensed by the instruments on board. Operation of the vernier engine at its highest thrust level will then bring the vehicle

to essentially zero velocity at zero altitude. Such a trajectory would not use the vernier engine during the first phase of the descent following main retro burnout. It is desirable, however, to use the vernier engine for attitude control during the entire powered descent, since stabilization by spinning is awkward for the sensing instruments, and since the possible misalignment of the main retro thrust is sufficient to require a sizable correcting moment to ensure proper attitude behavior.

Intermittent, on-off, operation of the vernier engine presents a problem in that continuous attitude control is needed, and also presents a greater reliability problem than does continuous operation which controls thrust level through a range between minimum and maximum thrust. In attitude control and reliability, then, the decision is to fall after main retro burnout at a minimum vernier thrust level of somewhat less than lunar weight. The known weight of the vehicle together with the maximum to minimum thrust ratio of a practical, liquid propellant vernier engine thus establishes the available thrust levels of the vernier engine in pounds.

The higher the maximum to minimum thrust ratio obtainable, the more efficient is the vernier descent. Beyond a certain value of this ratio, however, a variable injector area is necessary, whereas the more limited ratio obtainable by pressure control alone has the advantage in reliability of a proved design.

Thus, from consideration of the major characteristics of engines and instruments, a two-engine retro system is selected.

As is shown in Figure 2, the first main solid propellant engine removes the bulk of the velocity at a high constant level of thrust. A second, controllable, three-chamber, liquid propellant vernier engine controls vehicle attitude during the main retro engine, then operates at its minimum thrust following main retro burnout until a sensed velocity-altitude combination is reached such that maximum vernier thrust operation brings the vehicle to a speed of perhaps 10 feet per second at a few feet above the lunar surface. Then operation at a thrust level equal to lunar weight holds this low speed until impact, or allows the vehicle to drop in free fall for the last few feet. Thus the major characteristics of the retro system are decided.

For instrumentation, this engine system requires a range sensor for triggering the main retro at the proper altitude and a precision range sensor and velocity magnitude and direction sensor for monitoring the vernier descent phase both in thrust program and in attitude slaving of the thrust vector to the velocity direction.

Following a quantitative evaluation of the main retro errors and dispersions to be expected, it now is a matter of choosing the exact division of energy removal between the first and second engine such that the total retro system weight is least. The optimization procedure will answer the question, "At what nominal speed should the burnout of the main retro engine occur?"

2. MAIN RETRO ENGINE DISPERSIONS

For a vertical trajectory in which the thrust line is considered perfectly aligned to the vertical velocity, there are five sources of deviations which produce dispersions in the burnout altitude and velocity, two sources of initial conditions and three sources of engine conditions. Under the assumptions of a constant gravity field, Table 1 gives the equations for 1) the main retro descent, 2) the dispersions incurred during this descent, and 3) the minimum thrust and maximum thrust phases of the vernier descent considering vehicle mass constant during the vernier descent.

Figure 3 illustrates these error contributions, and the resulting ellipse represents dispersions in altitude and velocity. An altitude marking instrument provides the signal for ignition of the main retro engine. Error in this measurement results in error of burnout altitude only, in a constant gravity field, a closely approximate truth. Because of imperfect injection or midcourse correction conditions, an error in initial velocity is also present. This error produces a dispersion at burnout in both altitude and velocity, a correlated dispersion which contributes to the inclination of the dispersion ellipse. Note here that errors in velocity detected at midcourse of the same order of magnitude as the velocity dispersions of the main retro engine are better left uncorrected in the midcourse phase, since the particular velocity error to be contributed by the main retro engine is as yet unknown. Larger velocity corrections desired may be efficiently corrected at midcourse. It is pertinent

to mention here that the vernier engine logically performs the short period midcourse maneuver to correct injection errors which would result primarily in error in the lunar landing location.

A variation in the amount of main retro propellant loaded and of sliver behavior at burnout determines the exact amount of propellant burned and therefore contributes to variations in the burnout velocity, but has a negligible effect on the burnout altitude. Variation in the specific impulse, a variation in chemistry, affects total impulse by affecting thrust level. Such a variation also produces changes in both burnout velocity and altitude. Finally, variations in burning rate, as caused by grain shape deviations and more importantly by varying temperature of the propellant as affected by ambient launch pad and transit conditions cause changes in thrust level with essentially no change in total impulse. Their effect is therefore essentially limited to burnout altitude with little effect on burnout velocity.

Although not shown in Figure 3, if there is a variation in total vehicle weight at main retro ignition due to variation in the midcourse correction fuel consumed, the effect is similar to that caused by variation in both main engine fuel burned and in thrust level. This dispersion is handled automatically, however, if the nominal ignition weight is taken as corresponding to previous complete consumption of the midcourse fuel allowance. The heavier weight requiring more vernier descent fuel is due to having more vernier fuel available.

Table 1. Vertical Descent Equations

Definition of Symbols (in order of use)

$(\ )_o$	Value at start of main retro
$(\ )_1$	Value at end of main retro, start of minimum thrust vernier phase
$(\ )_2$	Value at end of minimum thrust vernier, start of maximum thrust vernier phase
V	Velocity, feet per second, negative when downward
h	Altitude, feet
c	Exhaust velocity ($I_{sp}G$), feet per second
W_p	Propellant weight consumed, pounds
W_o	Total initial spacecraft weight, pounds
g	Lunar surface gravity acceleration, 5.32 ft/sec^2, considered constant
G	Earth surface gravity acceleration, 32.2 ft/sec^2
T	Thrust, pounds
b	Ratio of maximum vernier thrust to lunar spacecraft weight
a	Ratio of minimum vernier thrust to lunar spacecraft weight
t	Time, seconds
m	Spacecraft mass, slugs, considered constant during vernier descent

Main Retro Descent

$$V_1 = V_o - c\left[\log(1 - W_p/W_o) + \frac{(W_p/W_o)(g/G)}{T/W_o}\right]$$

Table 1 (continued)

$$h_1 = h_o + \frac{c^2}{GT/W_o}\left\{(1 - W_p/W_o)\log(1 - W_p/W_o) + (W_p/W_o)\left[1 + V_o/c - \frac{(W_p/W_o)(g/G)}{2T/W_o}\right]\right\}$$

Main Retro Burnout Dispersions

$$\Delta V_1 = \Delta V_o + \frac{c(W_p/W_o)(g/G)}{T/W_o}\cdot\frac{\Delta(T/W_o)}{T/W_o} + cW_p/W_o\left[\frac{1}{1 - W_p/W_o} - \frac{g/G}{T/W_o}\right]\frac{\Delta(W_p/W_o)}{W_p/W_o} + (V_1 - V_o)\frac{\Delta c}{c}$$

$$\Delta h_1 = \Delta h_o + \frac{cW_p/W_o}{GT/W_o}\Delta V_o + \left[(g/2)\left(\frac{cW_p/W_o}{GT/W_o}\right)^2 + (h_o - h_1)\right]\frac{\Delta(T/W_o)}{T/W_o} + \frac{cV_1\,W_p/W_o}{GT/W_o}\frac{\Delta(W_p/W_o)}{W_p/W_o} - \left[2(h_o - h_1) + \frac{cV_o\,W_p/W_o}{GT/W_o}\right]\frac{\Delta c}{c}$$

Vernier Minimum Thrust Descent

$$V_2 = \mp\sqrt{\frac{b - 1}{b - a}\left[V_1^2 + 2gh_1(1 - a)\right]}$$

$$h_2 = h_1 - \frac{V_2^2 - V_1^2}{2g(1 - a)}$$

$$\left(\frac{W_p I_{sp}}{m}\right)_{\min T} = (a/1 - a)(V_1 - V_2)$$

Table 1 (continued)

Vernier Maximum Thrust Descent (ending at zero velocity and altitude)

$$V_2^2 = 2g(b - 1)h_2$$

$$\left(\frac{W_p I_{sp}}{m}\right)_{\text{max } T} = -V_2(b/b - 1)$$

Combined Vernier Minimum and Maximum Thrust Descent

$$\left(\frac{W_p I_{sp}}{m}\right)_{\text{Total}} = aV_1/1 - a + (1/1 - a)\sqrt{2gh_1\left(\frac{b - a}{b - 1}\right)(1 - a + V_1^2/2gh_1)}$$

3. VERNIER FUEL CONSUMPTION

For the purpose of illustrating the optimization procedure, Figure 4 shows the latter part of the descent trajectory under the assumption of a given lunar impact speed, at a larger scale than in the previous figures. The upper solid curve shows the end of the nominal main retro descent, and the ellipse shows the dispersions about the nominal. The lower solid curve represents the descent trajectory using maximum vernier thrust. The vehicle must never be allowed to descend into the altitude-velocity region, below and to the right of this curve, since in that region the maximum thrust of the vernier engine is too low to slow the vehicle to a soft landing speed before impact, regardless of the amount of vernier fuel available.

Loci of constant vernier fuel consumption are shown by each dashed curve. These curves indicate altitude-velocity combinations from which vehicle descent under the prescribed minimum and then maximum vernier thrust phases consumes a given constant amount of fuel. As indicated in Figure 4, the higher constant fuel curves represent more vernier fuel consumed. From the nominal burnout condition, the vehicle drops along the dot-dash curve at minimum vernier thrust to the solid curve. At this point, altitude and velocity sensors command maximum vernier thrust, and the vehicle follows this maximum thrust trajectory to approximately zero velocity at zero altitude. There is a point on the boundary of the dispersion ellipse, toward the upper right of the ellipse shown

in Figure 4, from which a descent consumes the maximum amount of vernier fuel corresponding to the particular nominal burnout condition illustrated.

4. OPTIMIZATION PROCEDURE

Consider the effect of moving the nominal burnout point and therefore the dispersion ellipse to the left from a location near the line of peaks of the constant vernier fuel curves. This move represents a main retro burnout at a slower speed and therefore requires more main retro fuel. From the shapes of the constant vernier fuel curves, it is apparent that this change also requires more vernier fuel. Clearly, such a main burnout region is undesirable. Consider, however, increasing the main burnout velocity, moving the ellipse to the right of the peaks of the constant vernier fuel curves. Again more vernier fuel is required, but now, with less velocity decrement during the main retro descent, less main retro fuel is needed. Thus in this region of main burnout speed, a compromise exists, indicating the possibility of an optimum main burnout velocity such that the total descent fuel required is least.

Figure 5 shows the change in main retro fuel, in vernier fuel, and in total fuel as a function of nominal main burnout velocity. Again the lunar approach, or rather impact speed, is considered constant. It is clear from Figure 5 that an optimum main burnout speed does in fact exist, one for which vernier fuel is at a minimum, more importantly one for which total descent fuel is at a minimum.

To avoid misunderstanding, it is emphasized that Figure 5 does not represent absolute weight values. The zeros of the different curves are different; only changes are shown.

Of course, it is least total retro system weight that is desired, rather than just descent fuel weight. As nominal main burnout velocity changes, so does main retro ignition altitude, and the initial altitude of vernier descent. These altitude changes have their effect on the range capability, and therefore weight, of the sensing instruments. More importantly, dry engine weight changes along with fuel capacity. Taking these changes into account, the curves of Figure 5 may be considered to represent change in fuel-plus-dry-engine weight and change in total retro system weight, including sensing instrumentation. Regarding Figure 5 in this light, it demonstrates that an optimum division of velocity removal between the first and second engine has been found such that total retro system weight is least. The optimization has been accomplished; the retro system is designed.

5. LAUNCH FLEXIBILITY

With the retro system defined, the velocity decrement of the main retro engine and the fuel capacity of the vernier engine are fixed. For an approximately constant transit time to the moon, determined by the locations on the earth of the launch site and the tracking facility, the lunar approach speed will vary, being in general greatest at lunar apogee and least at perigee. In addition, the varying lunar declination causes transit-time, and therefore approach-speed variations for earth-fixed visibility requirements.

For flexibility of launch time throughout the month, the vernier fuel capacity is chosen to handle the highest approach speed, and the optimization is performed for this most severe condition. For conditions other than apogee, the nominal main burnout will occur at a speed lower than that shown in Figure 5 corresponding to least total retro system weight. As nominal main burnout speed decreases, Figure 5 shows that vernier fuel required at first decreases, then rises again. The descent is still successful until such a low burnout speed is reached that the vernier fuel required is again equal to that for the design apogee condition. Within this range of nominal burnout speeds and therefore of approach speeds, which vary during the month, the vehicle retro system is flexible.

Should greater extension of the range at the low speed end be desired, it can be gained at some cost in simplicity. Depending on injection error, some vernier fuel may be available for an efficient midcourse velocity correction. Alternatively, since near perigee the injection velocity is lower, more weight can be injected, and a greater ignition weight would raise the nominal burnout speed. The selection of a main retro engine off-loaded by a few pounds would accomplish the same result.

6. EFFECT OF OFF-VERTICAL TRAJECTORIES AND ATTITUDES

It has been stated that the altitude and downward velocity of the vertical trajectory may be effectively considered as range and range rate for off-vertical trajectories. This is especially true if the thrust

vector is always closely aligned in opposition to the velocity vector. In that case, the trajectory direction changes very slowly during most of the descent and rotates to vertical only in the last, very low velocity phase. Moreover, as is assumed here, if the main retro thrust direction is held constant at the initial velocity direction at ignition, the trajectory changes appreciably from its initial direction only in the last few seconds of main retro operation. Velocity sensing and therefore servo aligning of the thrust vector to the instantaneous velocity vector during the main retro descent is difficult because of the dense, highly ionized exhaust products of the solid engine. The far lower thrust level and therefore less dense exhaust jet of the vernier engines is not expected to be troublesome to sensors, and velocity information during the vernier phase to servo the thrust in opposition to the velocity direction is relied upon. Should the velocity direction be more than perhaps 45° off-vertical at the end of main retro, however, the sensing of this fact and subsequent slaving of the vehicle (that is, thrust) attitude to this direction could result in such an extreme attitude that the velocity sensors no longer can perform their service for lack of view of the moon's surface.

To avoid this possibility, the full problem must be examined in which the velocity and thrust attitude direction are additional variables. In this case, the equations of motion are no longer integrable in closed form and machine computation becomes inevitable. The planar curves shown for example in Figure 4

in this discussion of vertical trajectories become three-dimensional surfaces; the dispersion ellipse becomes a dispersion footabll. The optimization procedure is very similar to that already described, but the mathematical techniques are more complicated and warrant a treatment of their own in Part II of this paper. Suffice it to say here that the effect of attitude errors and off-vertical trajectories show importance largely on the low end nominal burnout velocity cutoff.

PART II. A DIGITAL COMPUTER PROGRAM FOR OFF-VERTICAL TRAJECTORIES

1. MAIN RETRO DISPERSION ELLIPSOID

As in the case of the vertical trajectories discussed in Part I, the first step in computation for the off-vertical case is an evaluation of the dispersions at main retro burnout. For vertical trajectories, there were five sources of burnout dispersions, two in initial conditions and three in engine behavior. To these must now be added three new dispersion sources. The first is an error in the direction of the initial velocity at main retro ignition. The second is an error in the vehicle, and therefore thrust, attitude in that it is not perfectly aligned in opposition to the initial velocity. The third error results from the type of thrust attitude control assumed here.

In Part I no local sensing of the instantaneous velocity vector during main retro operation was assumed because of the difficulty of sensing through the dense exhaust jet. In Part II the thrust attitude is similarly considered constant at the initial velocity direction during the major portion of main retro operation. In order to set up the computations for the full range of possible variables, thus broadening the scope of the program, it is now assumed that at a few seconds before main burnout, local sensing and consequent slaving of the thrust attitude to the instantaneous velocity vector occurs. The third additional error, then, is a bias error in this continuous alignment of thrust to the changing velocity vector.

The eight sources of dispersion are listed as follows, in the order in which they are used in the following analysis:

$\Delta\theta_o$	Error in thrust attitude from initial velocity vector
$\Delta\theta_a$	Error in thrust attitude from instantaneous changing velocity vector
ΔV_o	Variation in velocity magnitude at ignition

ΔT	Variation in thrust due to propellant temperature variation
Δ_c	Variation in specific impulse (therefore also thrust)
Δt_1	Variation in burning time, equivalent to variation in propellant burned
Δh_o	Variation in ignition altitude
$\Delta \gamma_o$	Variation in velocity direction at ignition

Because of these eight perturbations, there are main retro dispersions in altitude, h, velocity magnitude, V, and now also in velocity direction, γ, thus forming a three-dimensional space. Each of these three dispersions is a variable dependent on the eight perturbations which are considered as random variables.

The random variables are assumed to be normally distributed and, pairwise, mutually independent. Nominal trajectories are run on the IBM 7090 for the various combinations of initial velocity orientation (relative to the horizontal) and retro terminal velocity magnitude: i.e., 10 or 20 cases, as required. For each of these nominal conditions, the variables as defined are perturbed one at a time, and the corresponding deviation from the nominal is obtained. Thus, the set of independent variables is reduced to three mutually dependent variables at the end of the first retro phase. These three are assumed to be jointly normally distributed. A confidence ellipsoid is then defined by the resulting three-dimensional normal distribution. In order to make this a 99 percent confidence interval, the quadratic form exponent is rotated to its normal form and the chi-squared distribution for three degrees of freedom is employed to establish the constant value for the exponent. This approach also establishes the semi-major axes and the orientation of the ellipsoid.

The equations of motion for $V > V_a$, where the thrust vector is fixed in space are given below and the geometry is shown in Figure 6.

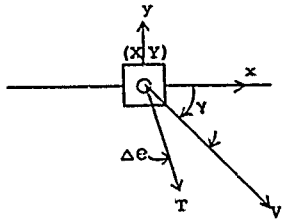

Origin is at position of initiation of main retro

Figure 6

(1) $a_y = \frac{T}{m} \sin(\gamma_o + \Delta\theta_o) - g$

(2) $a_x = -\frac{T}{m} \cos(\gamma_o + \Delta\theta_o)$

(3) $m = m_o - \frac{T}{c} t$

(4) $V_y = \int_o^{t_a} a_y \, dt - V_o \sin\gamma_o$

(5) $V_x = \int_o^{t_a} a_x \, dt + V_o \cos\gamma_o$

(6) $V = \sqrt{V_x^2 + V_y^2}$

(7) $y = \int_o^{t_a} V_y \, dt$

(8) $x = \int_o^{t_a} V_x \, dt$

γ_o = initial orientation angle

a_y = vertical acceleration

a_x = horizontal acceleration

m = instantaneous vehicle mass

V_y = vertical velocity

V_x = horizontal velocity

y = vertical displacement

x = horizontal displacement

γ_o, V_o, $\Delta\theta_o$, m_o are initial conditions

These equations of motion are employed until $V = V_a$, at which time the following equations are employed (see Figure 7). The initial conditions for these equations are the values of x, y, V_x, V_y, etc. at $V = V_a$.

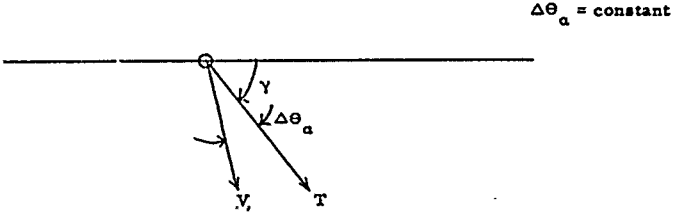

Figure 7

(9) $$a_y = \frac{T}{m} \sin (\gamma + \Delta\theta_a) - g$$

(10) $$a_x = -\frac{T}{m} \cos (\gamma + \Delta\theta_a)$$

(11) $$m = m_o - \frac{T}{c} t$$

(12) $$V_y = \int_{t_a}^{t_1} a_y \, dt - V_a \sin \gamma_a$$

(13) $$V_x = \int_{t_a}^{t_1} a_x \, dt - V_a \cos \gamma_a$$

(14) $$V = \sqrt{V_x^2 + V_y^2}$$

(15) $$\gamma = \tan^{-1} \left(-\frac{V_y}{V_x} \right)$$

$$(16) \qquad y = \int_{t_a}^{t_1} V_y \, dt + y_a$$

$$(17) \qquad x = \int_{t_a}^{t_1} V_x \, dt + x_a$$

This set of equations is solved simultaneously until $V = V_1$ -- some prescribed main retro terminal velocity. The time to reach V_1 is then observed, and the perturbation trajectories are run using this value of t_1.

From the above information and under the hypothesis of small perturbations, the variables h, V, and γ are defined as linear combinations of the eight perturbation variables previously listed. The perturbation notation is dropped for convenience--i.e., $\Delta\theta_o = \theta_o$, etc.

The various coefficients are the respective terminal, per unit perturbations from the ideal trajectory, a_i, b_i, and d_i.

$$(18) \qquad h = a_1\theta_o + a_2\theta_1 + a_3T + a_4c + a_5t_1 + a_6V_o + a_7h_o + a_8\gamma_o$$

$$(19) \qquad V = b_1\theta_o + b_2\theta_1 + b_3T + b_4c + b_5t_1 + b_6V_o + b_7h_o + b_8\gamma_o$$

$$(20) \qquad \gamma = d_1\theta_o + d_2\theta_1 + d_3T + d_4c + d_5t_1 + d_6V_o + d_7h_o + d_8\gamma_o$$

Since each of the independent variables of equations (18), (19), and (20) is Gaussian with known parameters, the parameters of the joint distribution can be determined for h, V, and γ. Thus,

$$(21) \qquad \sigma_h^2 = \sum_{i=1}^{8} a_i^2 \, \sigma_{x_i}^2$$

(22) $$\sigma_V^2 = \sum_{i=1}^{8} b_i^2 \sigma_{x_i}^2$$

(23) $$\sigma_\gamma^2 = \sum_{i=1}^{8} d_i^2 \sigma_{x_i}^2$$

where $x_i = \Theta_o, \Theta_1, T \ldots$ etc.

σ_{x_i} = standard deviation of the random variable x_i

(24) $$\rho_{hV} = \sum_{i=1}^{8} a_i b_i \sigma_{x_i}^2 / \sigma_h \sigma_V$$

(25) $$\rho_{V\gamma} = \sum_{i=1}^{8} b_i d_i \sigma_{x_i}^2 / \sigma_V \sigma_\gamma$$

(26) $$\rho_{\gamma h} = \sum_{i=1}^{8} d_i a_i \sigma_{x_i}^2 / \sigma_\gamma \sigma_h$$

ρ_{mn} = correlation coefficient between the m and n^{th} variable

$m, n = h, V, \gamma$

In terms of equations (21) through (26) and under the assumption that the joint distribution is Gaussian, this probability density is defined as

(27) $$\rho(h, V, \gamma) = \frac{\exp\left\{-\frac{1}{2|\Lambda|} \sum_{h,V,\gamma} \sum_{h,V,\gamma} |\Lambda|_{mn} (y_m)(y_n)\right\}}{(2\pi)^{3/2} |\Lambda|^{1/2}}$$

along with the covariance matrix equation (28).

$$(28) \qquad \Lambda = \begin{pmatrix} \sigma_h^2 & \rho_{hV}\,\sigma_h\,\sigma_V & \rho_{h\gamma}\,\sigma_h\,\sigma_\gamma \\ \rho V_h\,\sigma_V\,\sigma_h & \sigma_V^2 & \rho_{V\gamma}\,\sigma_V\,\sigma_\gamma \\ \rho_{\gamma h}\,\sigma_\gamma\,\sigma_h & \rho_{\gamma V}\,\sigma_\gamma\,\sigma_V & \sigma_\gamma^2 \end{pmatrix}$$

where

$|\Lambda|$ = determinant of the covariance matrix

$|\Lambda|_{mn}$ = cofactor of the m^{th} row and the n^{th} column term

y_m, y_n = h, V, γ

This distribution is considered in terms of 0 means for convenience. Once the confidence ellipsoid is established, it is located at its corresponding nominal point described above.

The exponent of the joint Gaussian distribution is a quadratic form and represents an ellipsoid in the h, V, γ space. The orientation and semi-major axes for this ellipsoid are illuminated by a coordinate rotation of this quadratic form into its normal coordinates, such that all cross-product terms of the exponent disappear. In terms of this new set of coordinates, the variables h', V', γ' are mutually and pairwise independent. Although not generally true, it is true for the Gaussian distribution that if the correlations between variables are zero, the variables are independent. Hence, the distribution in normal coordinates is a joint function of three independent variables.

Since they are expressed in terms of zero means and normalized relative to their respective variances, the three variables thus reduce to three independent normal variates of zero mean and unity variance. It is an established fact that the distribution of the sum of the squares of n independent normal variables of zero mean and unit variance is the chi-squared distribution with n degrees of freedom. Hence, after a rotation of the quadratic form to normal

coordinates the joint distribution is reduced to a chi-squared distribution of 3 d.f.

Let Q be the symmetrical matrix of the original quadratic form. Then Q can be reduced to diagonal form by some normalized orthogonal matrix $\mathcal{L}$

$$Q\mathcal{L} = \mathcal{L}K \tag{29}$$

where K is the diagonal matrix of eigen values for Q. It remains to solve for $\mathcal{L}$ and Q.

The solution of equation (29) leads to a set of simultaneous equations

$$\left.\begin{aligned} &(a_{11} - k_1) l_{11} + a_{12} l_{21} + \cdots a_{1n} l_{n1} = 0 \\ &a_{21} l_{12} + (a_{21} - k_2) l_{22} + \cdots a_{2n} l_{n2} = 0 \\ &\qquad\qquad \cdots \\ &a_{n1} l_{1n} + a_{n2} l_{2n} + \cdots (a_{nn} - k_n) l_{nn} = 0 \end{aligned}\right\} \tag{30}$$

where a_{ij} = element of Q

l_{ij} = element of $\mathcal{L}$

k_i = element of K

This set of equations has a non-trivial solution only if

$$\begin{vmatrix} a_{11} - k & a_{12} & \cdots & a_{1n} \\ a_{21} & a_{22} - k & \cdots & a_{2n} \\ & \cdots & & \\ a_{n2} & \cdots & & a_{nn} - k \end{vmatrix} = 0 \tag{31}$$

which leads to an n^{th} order plynomial in k. In matrix notation this reads $|Q - K| = 0$.

Thus, from equation (27) the quadratic form is

$$(32)\quad |\Lambda|_{hh}\, h^2 + |\Lambda|_{VV}\, v^2 + |\Lambda|_{\gamma\gamma}\, \gamma^2 - 2|\Lambda|_{hV}\, hV - 2|\Lambda|_{V\gamma}\, V\gamma - 2|\Lambda|_{\gamma h}\, \gamma h = k$$

where the constant k is established in order to make this ellipsoidal volume a 99 percent (3σ) confidence interval.

The direction numbers for this quadratic form are established by means of the following set of equations, i = 1, 2, 3.

$$\begin{pmatrix} |\Lambda|_{hh} - k_i & |\Lambda|_{hV} & |\Lambda|_{h\gamma} \\ |\Lambda|_{hV} & |\Lambda|_{VV} - k_i & |\Lambda|_{V\gamma} \\ |\Lambda|_{h\gamma} & |\Lambda|_{V\gamma} & |\Lambda|_{\gamma\gamma} - k_i \end{pmatrix} \begin{pmatrix} \ell_i \\ m_i \\ n_i \end{pmatrix} = \begin{pmatrix} 0 \\ 0 \\ 0 \end{pmatrix}$$

where the k_i are the eigen values for the quadratic form and are computed from the third degree polynomial.

$$(34)\quad \begin{vmatrix} |\Lambda|_{hh} - k_i & |\Lambda|_{hV} & |\Lambda|_{h\gamma} \\ |\Lambda|_{hV} & |\Lambda|_{VV} - k_i & |\Lambda|_{V\gamma} \\ |\Lambda|_{h\gamma} & |\Lambda|_{V\gamma} & |\Lambda|_{\gamma\gamma} - k_i \end{vmatrix} = 0$$

Hence for each k_i, a triple ratio $\ell_i/m_i/n_i$ of direction numbers is obtained, where each such set defines the direction of one of the normal coordinates.

From a chi-squared distribution table, it is found that k = 11.341 for 3 d.f. and the quadratic surface in nominal coordinates (h_t, V_h, γ_h) is

$$k_1 h_n^2 + k_2 V_n^2 + k_3 \gamma_n^2 = 11.341 \tag{35}$$

or

$$\frac{\left(\frac{h_n}{3}\right)^2}{\frac{11.341}{9k_1}} + \frac{\left(\frac{V_n}{3}\right)^2}{\frac{11.341}{9k_2}} + \frac{\left(\frac{\gamma_n}{3}\right)^2}{\frac{11.341}{9k_3}} = 1 \tag{36}$$

Thus, the 99 percent confidence ellipsoid is defined. It has a canonic form relative to the coordinate system defined by equation (37):

$$\begin{pmatrix} \ell_1 & \ell_2 & \ell_3 \\ m_1 & m_2 & m_3 \\ n_1 & n_2 & n_3 \end{pmatrix} \tag{37}$$

and the semi-major axes in terms of 3σ values are

$$(3\sigma_{hn})^2 = \frac{11.341}{9k_1} \tag{38}$$

$$(3\sigma_{Vn})^2 = \frac{11.341}{9k_2} \tag{39}$$

$$(3\sigma_{\gamma n})^2 = \frac{11.341}{9k_3} \tag{40}$$

As an illustration of the above theory, it will be applied to the two-dimensional case where $\gamma = 0$.

$$(41) \qquad \rho(h,V) = \frac{\exp\left[-\frac{1}{2|\Lambda|}\sum_{n}^{2}\sum_{m}^{2}|\Lambda|_{mn}\, y_n y_m\right]}{(2\pi)^{2/2}\,|\Lambda|^{1/2}}$$

where $m_h = m_H = 0$

$$(42) \qquad \Lambda = \begin{vmatrix} \sigma_n^2 & \rho_{hV}\,\sigma_h\sigma_V \\ \rho_{Vh}\,\sigma_n\sigma_V & \sigma_Y^2 \end{vmatrix}$$

$$(43) \qquad |\Lambda| = \sigma_h^2\sigma_V^2 - \rho_{hV}^2\sigma_h^2\sigma_V^2 = \sigma_h^2\sigma_V^2\,(1-\rho_{hV}^2)$$

Q = Quadratic form

$$(44) \qquad Q = \frac{1}{2\sigma_h^2\sigma_V^2(1-\rho_{hV})}\left[|\Lambda|_{hh}\,h^2 + |\Lambda|_{hV}\,hV + |\Lambda|_{Vh}\,Vh + |\Lambda|_{VV}\,V^2\right]$$

$$(45) \qquad \begin{aligned} |\Lambda|_{hh} &= \sigma_V^2 \\ |\Lambda|_{hV} &= -\rho_{Vh}\,\sigma_h\sigma_V \\ |\Lambda|_{V_h} &= -\rho_{hV}\,\sigma_h\sigma_V \\ |\Lambda|_{VV} &= \sigma_h^2 \end{aligned}$$

or

$$(46) \qquad Q = -\frac{1}{2(1-\rho^2)\,\sigma_h^2\sigma_V^2}\,(\sigma_V^2\,h^2 - 2\rho\,\sigma_h\sigma_V hV + \sigma_h^2\,V^2)$$

Solving for the eigen values, in terms of the determinant for the matrix of cofactors,

$$(47) \qquad \begin{vmatrix} \sigma_V^2 - k & -\rho\,\sigma_h\sigma_V \\ -\rho\,\sigma_h\sigma_V & \sigma_h^2 - k \end{vmatrix} = 0$$

$$(48) \qquad k = \frac{(\sigma_h^2 + \sigma_V^2 \pm \sqrt{(\sigma_h^2 - \sigma_V^2)^2 + 4\sigma_V\sigma_h^2\rho^2}}{2}$$

Now solve for the normal directions of the ellipse:

$$(49) \qquad \begin{pmatrix} \sigma_V^2 - k & -\rho\,\sigma_h\sigma_V \\ -\rho\,\sigma_h\sigma_V & \sigma_h^2 - k \end{pmatrix} \begin{pmatrix} \ell \\ m \end{pmatrix} = \begin{pmatrix} 0 \\ 0 \end{pmatrix}$$

$$(50) \qquad \left.\begin{aligned} (\sigma_V^2 - k)\,\ell \;-\; & \rho\,\sigma_h\sigma_V m = 0 \\ -\rho\,\sigma_h\sigma_V\ell \;+\; & (\sigma_h^2 - k)m = 0 \end{aligned}\right\} \quad \text{for } k = k_1,\ k_2$$

$$(51) \qquad \begin{aligned} (\sigma_V^2 - k)\,\ell &= +\rho\,\sigma_h\sigma_V m \\ \rho\,\sigma_h\sigma_V\ell &= +(\sigma_h^2 - k)m \end{aligned}$$

$$(52) \qquad \ell/m = \frac{+\rho\,\sigma_h\sigma_V}{\sigma_V^2 - k} = \frac{\sigma_h^2 - k}{\rho\,\sigma_h\sigma_V}$$

Either relation will lead to the same result. The direction cosines for the normal coordinates are therefore the elements of the following transformation matrix.

$$(53) \qquad \begin{pmatrix} h_1 \\ V_1 \end{pmatrix} = \begin{pmatrix} \frac{\ell_1}{N_1} & \frac{\ell_2}{N_2} \\ \frac{m_1}{N_1} & \frac{m_2}{N_2} \end{pmatrix} \begin{pmatrix} h \\ V \end{pmatrix}$$

where h and V are components of a vector relative to the original coordinates, and h' and V' are the components of the same vector relative to the normal coordinates.

Define:

$$(54) \qquad \begin{cases} \frac{\ell_2}{N_2} = \frac{\rho\, \sigma_h \sigma_V}{\sqrt{(\sigma_V^2 - k_1)^2\, \rho^2\, \sigma_h^2\, \sigma_V^2}} \\ \frac{m_2}{N_2} = \frac{\sigma_V^2 - k_1}{\sqrt{(\sigma_V^2 - k_1)^2 + \rho^2\, \sigma_h^2\, \sigma_V^2}} \\ \frac{\ell_1}{N_2} = \frac{\sigma_h^2 - k_2}{\sqrt{(\sigma_h^2 - k_2)^2 + \rho\, \sigma_h^2\, \sigma_V^2}} \\ \frac{m_1}{N_2} = \frac{\rho\, \sigma_h\, \sigma_V}{\sqrt{(\sigma_h^2 - k_2)^2 + \rho^2\, \sigma_h^2\, \sigma_V^2}} \end{cases}$$

Hence

$$\tan\Theta = -\frac{m_1}{l_1} = -\frac{(\sigma_h^2 - k_2)}{\rho\,\sigma_h\,\sigma_V} \tag{55}$$

for a counterclockwise rotation from the h, V axes (see Figure 8).

$$\sigma_h^2 - k_2 = \frac{\sigma_h^2}{2} - \frac{\sigma_V^2}{2} + \frac{\sqrt{(\sigma_h^2 - \sigma_V^2)^2 + 4\rho^2\,\sigma_h^2\,\sigma_V^2}}{2}$$

where

$$k_2 = \frac{(\sigma_h^2 + \sigma_V^2) - \sqrt{(\sigma_h^2 - \sigma_V^2)^2 + \sigma_V^2\,\sigma_h^2\,\rho^2}}{2}$$

Hence

$$\tan\Theta = -\frac{(\sigma_h^2 - k_1)}{\rho\,\sigma_h\sigma_V} = -\left\{\frac{\sigma_h^2 - \sigma_h^2}{2\rho\,\sigma_h\sigma_V} + \sqrt{\frac{(\sigma_h^2 - \sigma_V^2)^2}{4\rho^2\,\sigma_h^2\sigma_V^2}} + 1\right\} \tag{56}$$

Let

$$\tan 2\Theta = \frac{2\tan\Theta}{1 - \tan^2\Theta}$$

$$a = \frac{(\sigma_h^2 - \sigma_V^2)}{2\rho\,\sigma_h\sigma_V}$$

therefore

$$\tan\Theta = -\left(a + \sqrt{a^2 + 1}\right)$$

and

$$\tan 2\Theta = \frac{-2(a + \sqrt{a^2 + 1})}{-(2)(a^2 + a\sqrt{a^2 + 1})} = \frac{1}{a}$$

thus

(57) $$\tan 2\theta = \frac{2\rho\,\sigma_h\sigma_V}{\sigma_h^2 - \sigma_V^2}$$

Define:

$$\mathcal{L} = \begin{pmatrix} \frac{\ell_1}{N_1} & \frac{\ell_2}{N_2} \\ \frac{m_1}{N_1} & \frac{m_2}{N_2} \end{pmatrix}$$

$$\mathcal{L}^{-1} = \begin{pmatrix} \frac{\ell_1}{N_1} & \frac{m_1}{N_1} \\ \frac{\ell_2}{N_2} & \frac{m_2}{N_2} \end{pmatrix}$$

since $\mathcal{L}$ is a normalized orthogonal matrix

Therefore $$\mathcal{L}^{-1} \begin{pmatrix} \sigma_V^2 & -\rho_{VH}\,\omega_h\sigma_V \\ -\rho_{Vh}\,\sigma_h\sigma_V & \sigma_h^2 \end{pmatrix} \mathcal{L} = \begin{pmatrix} k_1 & 0 \\ 0 & k_2 \end{pmatrix}$$

Hence

(58) $$Q' = -\frac{1}{2|\Lambda|}\left[k_1 h_1^2 + k_2 V_1^2\right]$$

For 2 d.f. we find rom the chi-squared table that the exponent k should be 9.937 in order that the dispersion ellipse include 99 percent of all dispersions from the nominal point at main retro burnout. Thus,

(59) $$k_1 h_1^2 + k_2 V_1^2 = 9.937$$

$$\frac{k_1 h_1^2/(9)}{9.937/(9)} + \frac{k_2 V_1^2/9}{9.937/(9)} = 1$$

Divide both numerator and denominator by 9 in both terms to force the semi-major axes of the dispersion ellipse to be 3σ values. Hence, the semi-major axes about the nominal point are:

(60) $$(3\sigma_{h_1}) = \frac{9.937}{9k_1} \quad \text{and} \quad (3\sigma_{V_1}) = \frac{9.937}{9k_2}$$

See Figure 8.

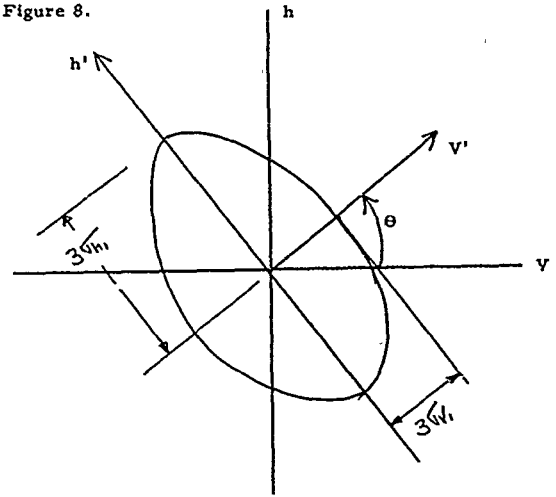

Dispersion Ellipse
Figure 8

2. MAXIMUM VERNIER THRUST SURFACE

The maximum vernier thrust surface is defined as the surface of points in the h, V, γ space, from which the vehicle can come to a zero altitude zero velocity landing, if retroed at the maximum vernier thrust. The equations of motion for this phase of the trajectory are (assuming constant mass):

$$a_y = -g\left(b\frac{V_y}{V} + 1\right) \tag{58}$$

$$a_x = -g\,b\frac{V_x}{V} \tag{59}$$

$$V_y = \int_o^t a_y\,dt - V_2 \sin\gamma_2 \tag{60}$$

$$V^2 = V_x^2 + V_y^2 \tag{61}$$

$$V_x = \int_o^t a_x\,dt + V_2\cos\gamma_2 \tag{62}$$

$$y = \int_o^t V_y\,dt \tag{63}$$

$$x = \int_o^t V_x\,dt \tag{64}$$

a_i, i=x, y Acceleration, ft/sec^2

g Lunar gravity, ft/sec^2

b Maximum vernier thrust/lunar weight ratio

V_i, i=x, y Velocity, ft/sec

x, y Displacement, feet

This set of equations is solved simultaneously until $V_y = 0$. At this time, $h_2 = -y$. In this way a number of discrete points on the surface are determined. Then, by means of a curve fitting process, a smooth curve can be found to satisfy all points found.

For the data run to date, a surface that approximates all data points to within 3 percent is

(64) $$h_2 = \frac{V_2^2}{2g\left[\frac{b}{2}\left(1 + \frac{1}{\sin \gamma_2}\right) - 1\right]}$$

The time for descent is found in a similar fashion and is

(65) $$t_2 = \frac{V_2/g}{\frac{b}{6.5}\left[\frac{1}{\sin \gamma_2} + 5.5\right] - 1}$$

3. SURFACE OF NOMINAL MAIN BURNOUT CONDITIONS

Having defined the distribution ellipse, E, and the surface, S_2, in the h_1 V_1 γ_1 space, a surface of nominal points can be established. This surface is a locus of main retro burnout points under ideal conditions, i.e., zero error perturbations.

This surface is established by finding the centers of the ellipsoids which are tangent to the S_2 surface.

(66) $$h_2 = \frac{V_2^2/g}{b\,(1 + 1/\sin \gamma_2) - 2}$$

(67) $$\begin{aligned} &\Lambda_{hh}(h_2 - h_n)^2 + \Lambda_{VV}(V_2 - V_n)^2 + \Lambda_{\gamma\gamma}(\gamma_2 - \gamma_n)^2 \\ &+ 2\Lambda_{hV}(h_2 - h_n)(V_2 - V_n) + 2\Lambda_{h\gamma}(h_2 - h_n)(\gamma_2 - \gamma_n) \\ &+ 2\Lambda_{V\gamma}(V_2 - V_n)(\gamma_2 - \gamma_n) - 1.26 = 0 \end{aligned}$$

Equations (66) and (67) represent the maximum vernier thrust surface and the elliptical surface in terms of a nominal center, (h_n, V_n, γ_n), and their point of tangency, (h_2, V_2, γ_2). In addition, the slopes of the two surfaces, in the h-V plane and h-γ plane must also be equal. These latter relations are described by equations (68) and (69).

(68) $$\frac{2h_2}{V_2^2} + \frac{\Lambda_{VV}(V_2 - V_n) + \Lambda_{hV}(h_2 - h_n) + \Lambda_{V\gamma}(\gamma_2 - \gamma_n)}{\Lambda_{hh}(h_2 - h_n) + \Lambda_{hV}(V_2 - V_n) + \Lambda_{h\gamma}(\gamma_2 - \gamma_n)} = 0$$

(69) $$\frac{g}{57.3}\frac{h_2^2}{V_2^2}\frac{\cos \gamma_2}{\sin^2 \gamma_2} + \frac{\Lambda_{\gamma\gamma}(\gamma_2 - \gamma_n) + \Lambda_{h\gamma}(h_2 - h_n) + \Lambda_{V\gamma}(V_2 - V_n)}{\Lambda_{hh}(h_2 - h_n) + \Lambda_{hV}(V_2 - V_n) + \Lambda_{h\gamma}(\gamma_2 - \gamma_n)} = 0$$

Equations (66), (67), (68), and (69) are solved simultaneously by assuming values for V_2 and γ_2, and solving for h_2, h_n, V_n, and γ_n under the condition that $h_n > h_2$.

The symbols employed here have been defined previously. The surface of nominal points can then be established by means of a curve fitting procedure, or the data points can merely be stored as such for future use. This surface (or points) shall hereafter be referred to as the S_{1_n} surface.

4. SURFACES OF CONSTANT VERNIER FUEL

The surface of constant vernier fuel is established by integrating the equations of motion during the drift period (minimum vernier thrust) backwards (negative time) using the points of S_2 as initial conditions.

(70) $$t_1 = \frac{C - m_2 t_2}{m_1}$$

t_1 = time for minimum vernier thrust phase, seconds

t_2 = time for maximum vernier thrust phase, seconds (see equation (65))

$\dot{m}_1$ = minimum thrust mass flow rate, slugs/sec (a constant)

$\dot{m}_2$ = maximum thrust mass flow rate, slugs/sec (a constant)

C = total vernier fuel mass, slugs

(71) $$V_y = \int_o^{t_1} g \left(a \frac{V_y}{V} + 1\right) dt - V_2 \sin \gamma_2$$

(72) $$V_x = \int_o^{t_1} g\, a \frac{V_x}{V}\, dt + V_2 \cos \gamma_2$$

(73) $$V = \sqrt{V_x^2 + V_y^2}$$

(74) $$h = \int_o^{t_1} - V_y \, dt + h_2$$

(75) $$\gamma_2 = \tan^{-1}\left(\frac{-V_y}{V_x}\right)$$

where h_2 is defined by equation (64).

For every value of h_2, V_2 and γ_2 a t_2 is defined, (see equation (65)). Hence, every value C establishes a t_1, a minimum vernier drift time. Integrating equations (70) through (75) yields points (h_f, V_f, γ_f), for various values of C. By curve fitting these points S_f is established, with C as a parameter.

(76) $$h_f = \frac{1}{2g\,(1-a)}\left\{\frac{b'-1}{b'-a}\left[(1-a)\,\frac{C\,W_p}{W_v} + a\,V'\right] - V'^2\right\}$$

W_p = vernier fuel weight

W_v = average vehicle weight during vernier descent

where

(77) $$b' = b - 0.57\,(1 - \sin\gamma_f)$$

(78) $$V' = V_f\,[\,1 - 0.38\,(1 - \sin\gamma_f)\,]$$

5. INTEGRATION OF THE COMPUTER PROGRAM

The IBM programs for the various surfaces:

E = dispersion ellipsoids

S_{1_n} = surface of nominal points

S_2 = surface of maximum vernier fuel

S_f = surface of constant vernier fuel ,

are integration into a master program. This master program accepts any set of perturbations and initial conditions as inputs and establishes the various surfaces defined above.

The total fuel is then optimized as a function of main retro terminal velocity in the following manner:

1) A set of main retro terminal conditions establishes a dispersion ellipsoid center and surface.
2) A computer search is then made for the point of tangency of this ellipsoid and the S_f surface. This is done

by finding the intersections of E and S_f for various values of h_1 and C. When an S_f surface is found (identified by C) such that its intersection with the ellipsoid is one point, the search ends. This point of tangency represents the maximum required amount of vernier fuel required corresponding to the chosen nominal point.

3) The total engine weight is then computed as

(79) $$k_m M_m + K_v C = M_T$$

k_m = ratio of total main retro engine weight to its propellant weight

K_V = ratio of total vernier engine weight to its propellant weight

M_T = total engine weight

4) Curves of $k_m M_m$ and $K_V C$ versus nominal main retro terminal velocity V_T, are generated by repeated computer runs for a range of desirable values for V_T. The sum of the two engine weights is characterized by a minimum at some nominal main retro terminal velocity. This value of terminal velocity represents the optimum in the trade-off of energy removal during the main retro and vernier phases as discussed at the end of Part I. The above program is integrated so that a given set of perturbations and initial conditions will result in an engine system design of least weight.

CONCLUSION

In summary, broad considerations of simplicity and reliability, and hardware trade-offs involving accuracy and weight, have led to the choice of a two-engine retro system for the slowdown from lunar approach speed to a soft landing speed. Within the system limitations imposed by the practical propulsion and sensing techniques existing today, an optimization procedure has divided the energy removal between the two engines such that total retro system weight is least. A digital computer program for the optimization in the case of off-vertical trajectories has also been detailed.

Should the available engine and sensor techniques change, and they will, the answers shown and implied here will also change. But it seems that the broad design approach and the optimization procedure will remain valid and that their use with different inputs will produce new, correct, different results.

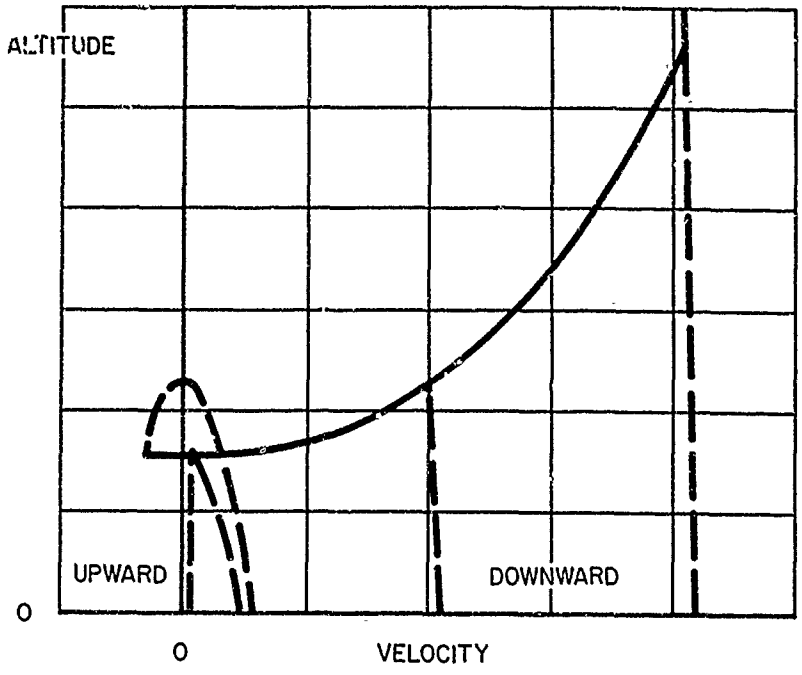

FIGURE 1 SAMPLE DESCENT TRAJECTORIES

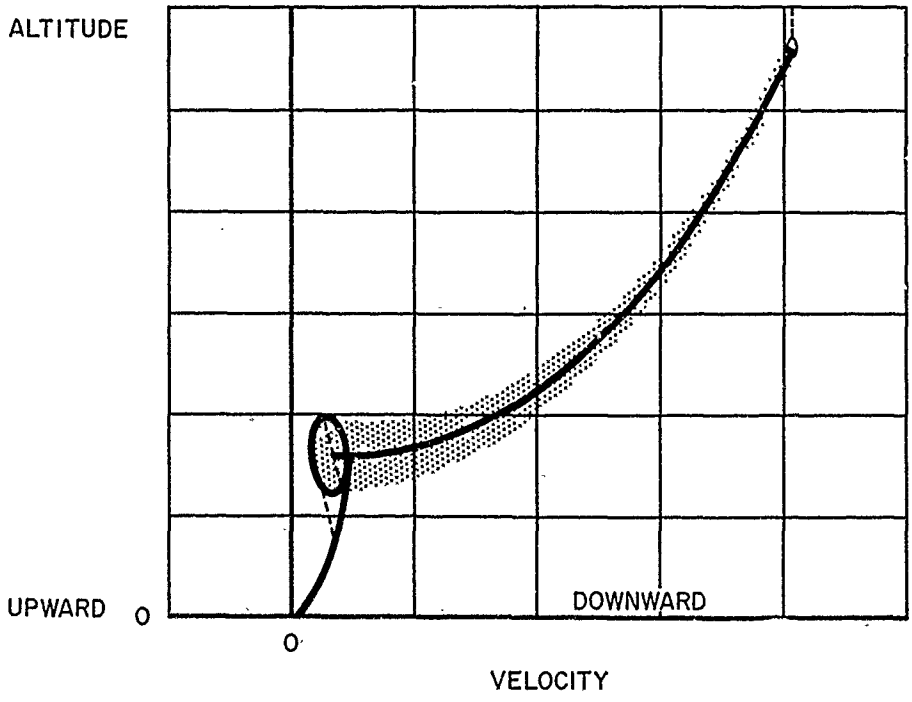

FIGURE 2 DESIGN DESCENT TRAJECTORY

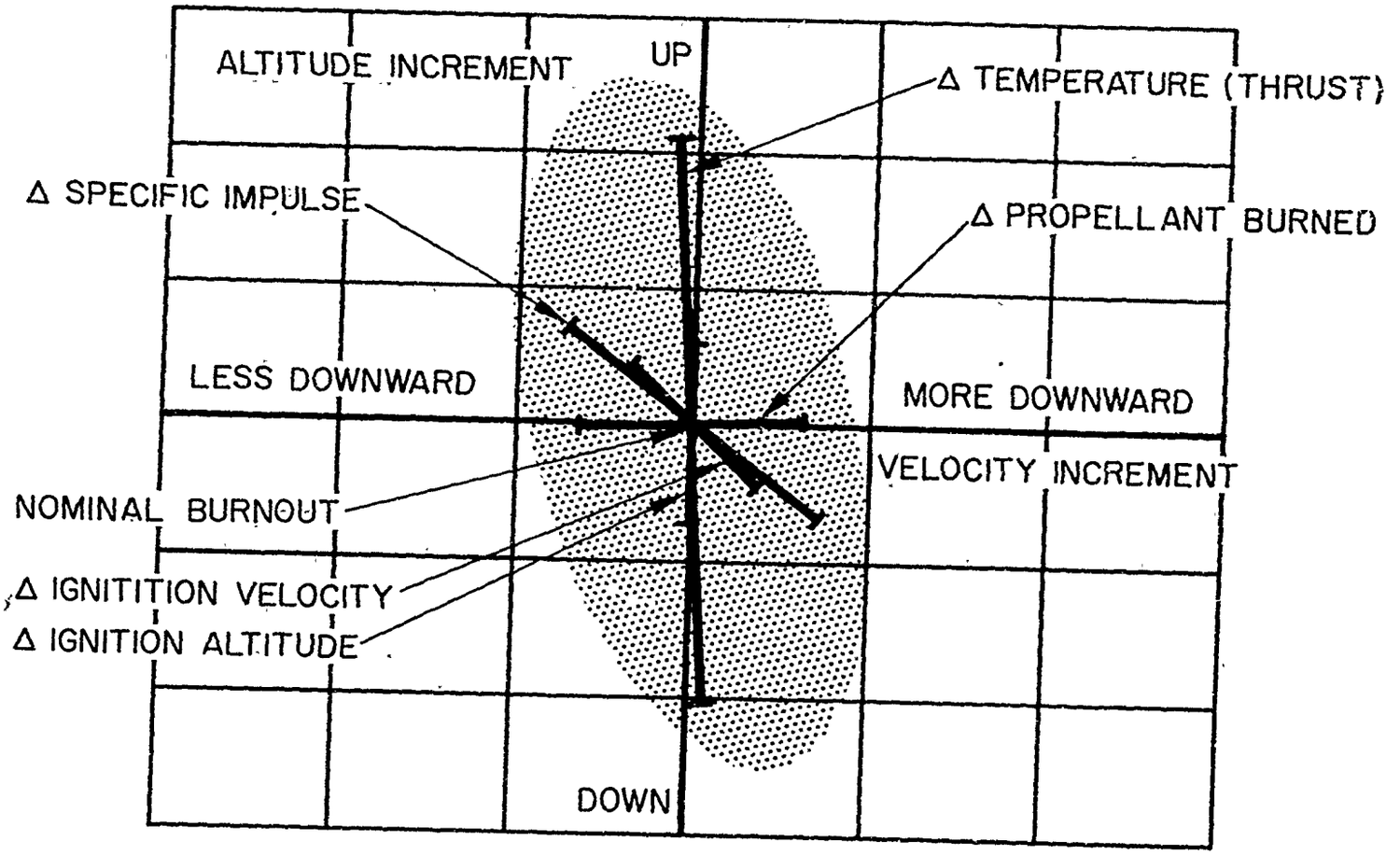

FIGURE 3 MAIN RETRO ENGINE BURNOUT DISPERSIONS

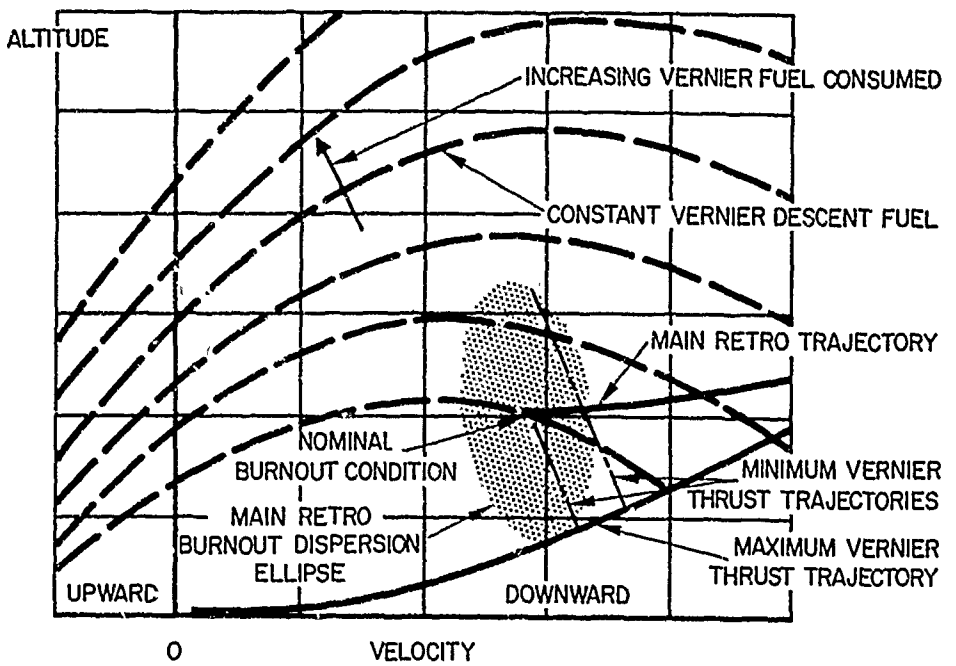

FIGURE 4 VERNIER ENGINE DESCENT AND VERNIER FUEL

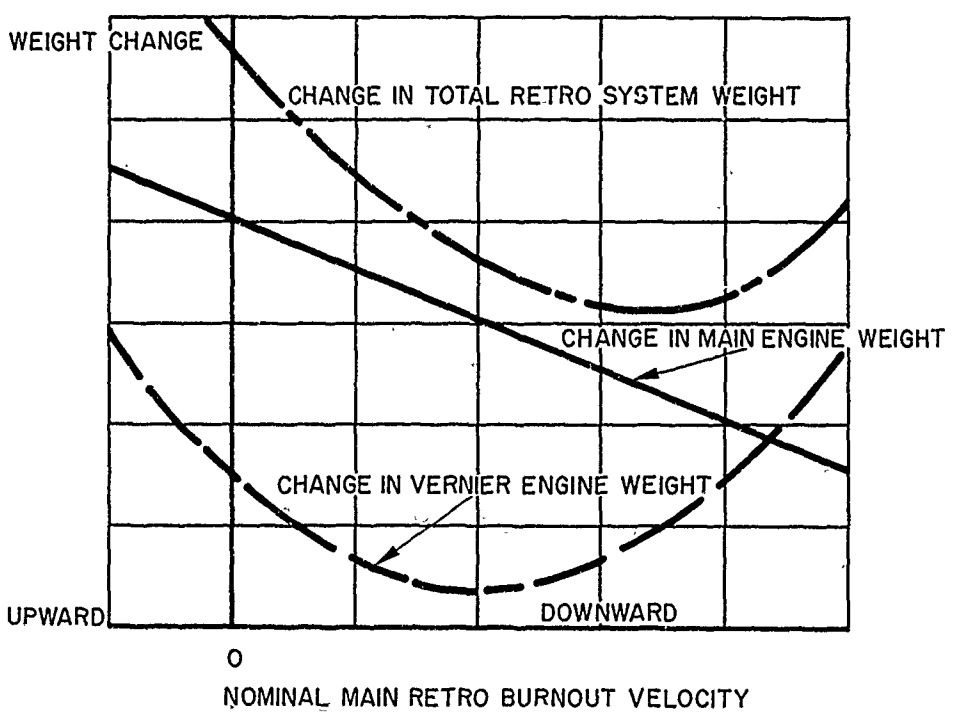

FIGURE 5 CHANGE IN FUEL AND SYSTEM WEIGHTS